A Generalization of Poiseuille's Law for the Flow of a Self-Similar (Fractal) Fluid through a Tube Having a Fractal Rough Surface

Abdellah Bouchendouka, Zine El Abiddine Fellah, Zakaria Larbi, Nicholas O Ongwen, Erick Ogam, Mohamed Fellah, Claude Depollier

fractal and fractional

MDPI

Article

A Generalization of Poiseuille's Law for the Flow of a Self-Similar (Fractal) Fluid through a Tube Having a Fractal Rough Surface

Abdellah Bouchendouka [1], Zine El Abiddine Fellah [1,*], Zakaria Larbi [2], Nicholas O. Ongwen [3], Erick Ogam [1], Mohamed Fellah [4] and Claude Depollier [5]

[1] Aix Marseille Univ, CNRS, Centrale Marseille, LMA UMR 7031, Marseille, 4 Impasse Nikola Tesla CS 40006, CEDEX 13, 13453 Marseille, France
[2] Laboratory of Theoretical and Applied Fluid Mechanics, Physics' Faculty, University of Sciences and Technology Houari Boumediene USTHB, LMFTA BP 32 El Alia, Bab Ezzouar 16111, Algiers, Algeria
[3] Department of Physics and Materials Science, Maseno University, Maseno 40105, Kenya
[4] Laboratory of Theoretical Physics, Faculty of Physics, University of Sciences and Technology Houari Boumediene USTHB, BP 32 El Alia, Bab Ezzouar 16111, Algiers, Algeria
[5] Laboratoire d'Acoustique de l'Université du Mans (LAUM), UMR 6613, Institut d'Acoustique-Graduate School (IA-GS), CNRS, Le Mans Université, Avenue O. Messiaen, CEDEX 09, F-72085 Le Mans, France
* Correspondence: fellah@lma.cnrs-mrs.fr

Abstract: In this paper, a generalization of Poiseuille's law for a self-similar fluid flow through a tube having a rough surface is proposed. The originality of this work is to consider, simultaneously, the self-similarity structure of the fluid and the roughness of the tube surface. This study can have a wide range of applications, for example, for fractal fluid dynamics in hydrology. The roughness of the tube surface presents a fractal structure that can be described by the surface fractal noninteger dimensions. Complex fluids that are invariant to changes in scale (self-similar) are modeled as a continuous medium in noninteger dimensional spaces. In this work, the analytical solution of the Navier–Stokes equations for the case of a self-similar fluid flow through a rough "fractal" tube is presented. New expressions of the velocity profiles, the fluid discharge, and the friction factor are determined analytically and plotted numerically. These expressions contain fractal dimensions describing the effects of the fractal aspect of the fluid and of that of the tube surface. This approach reveals some very important results. For the velocity profile to represent a physical solution, the fractal dimension of the fluid ranges between 0.5 and 1. This study also qualitatively demonstrates that self-similar fluids have shear thickening-like behavior. The fractal (self-similarity) nature of the fluid and the roughness of the surface both have a huge impact on the dynamics of the flow. The fractal dimension of the fluid affects the amplitude and the shape of the velocity profile, which loses its parabolic shape for some values of the fluid fractal dimension. By contrast, the roughness of the surface affects only the amplitude of the velocity profile. Nevertheless, both the fluid's fractal dimension and the surface roughness have a major influence on the behavior of the fluid, and should not be neglected.

Keywords: self-similar fluid; noninteger dimensional spaces; fractal tube surface; Poiseuille's law; surface fractal dimensions, Navier–Stokes equations for fractal medium

Citation: Bouchendouka, A.; Fellah, Z.E.A.; Larbi, Z.; Ongwen, N.O.; Ogam, E.; Fellah, M.; Depollier, C. A Generalization of Poiseuille's Law for the Flow of a Self-Similar (Fractal) Fluid through a Tube Having a Fractal Rough Surface. *Fractal Fract.* **2023**, *7*, 61. https://doi.org/10.3390/fractalfract7010061

Academic Editor: Haci Mehmet Baskonus

Received: 17 October 2022
Revised: 6 December 2022
Accepted: 22 December 2022
Published: 4 January 2023

1. Introduction

A medium that exhibits fractal properties has a structure that remains unchanged when lengths are uniformly scaled, meaning that a fractal medium (or object) appears, statistically, similar at different scales (see Figure 1). This self-similarity appears almost everywhere in nature, from the lungs of a human being to the galaxies of outer space. Fractal objects have characteristics that remain unchanged regardless of the scale at which they are observed, and these features can be described using dimensions that are not whole numbers [1].

According to Mandelbrot [1,2], these fractal dimensions can give a better understanding of turbulence, star distribution, galaxies, and so on. Fractal methods have become increasingly popular in recent years and have the potential to be useful in a variety of fields and contexts including biology and medicine [3,4], geology and earth sciences [5,6], image analysis [7,8], astronomy [9,10], and acoustics [11–15]. Fluids and rough surfaces which are the scope of our study also exhibit a self-similar "fractal" structure. Examples of self-similar "fractal" fluids include fractal emulsions in which a fluid is fractally dispersed in another fluid [16], fractal solutions, with a fractal distribution of a solute dissolved in a nonfractal solvent [17], fractal suspensions in which a solid is fractally distributed in a fluid [18]. Several researchers have developed models for examining fractal fluids in noninteger dimensional spaces (NIDS), including Ostoja-Starzewski [19–22], Balankin [23–25], and Tarasov [26,27]. This article considers the method proposed by Tarasov [26].

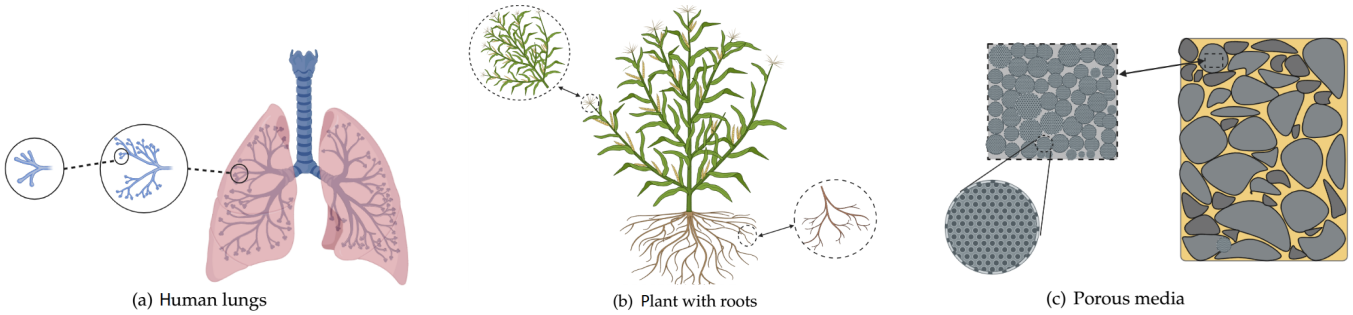

Figure 1. Examples of objects that display a self-similar "fractal" structure.

Vector calculus in spaces with noninteger dimensions is widely used in various fields, e.g., to regularize ultraviolet divergences in quantum field theory [28,29] and to study critical phenomena and phase transitions in statistical physics [30,31]. Tarasov [26] proposed a way to extend vector calculus to spaces with noninteger dimensions, defining first- and second-order operators such as the gradient, divergence, scalar and vector Laplace operators. These operators can be used to reformulate the Navier–Stokes equations for a fractal Newtonian incompressible fluid flow [27,32]. For a self-similar fluid, the mass of a region of the fluid enclosed within a ball of radius R follows a power-law relation of the form $M \propto R^D$ [26], where D is a noninteger dimension of a fluid particle [26,33]. The fractal dimension D reflects the degree to which the fluid fills the Euclidean space in which it exists. For a self-similar viscous fluid, $D < 3$, while for a viscous fluid, $D = 3$ (see Figure 2). The power-law relationship $M \propto R^D$ can be derived through the use of integrations in noninteger dimensional spaces (see ref. [33] for more details).

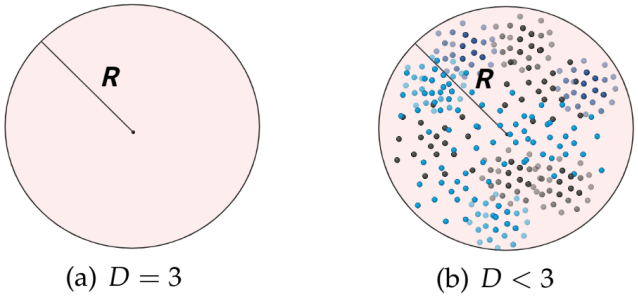

Figure 2. Schematic of a ball region of a fluid with radius R: (**a**) viscous fluid; (**b**) self-similar viscous fluid.

For tubes with a radius less than a few millimeters, the roughness of the surface plays a significant role and cannot be neglected. According to Brown [34], factors that influence the flow of a fluid through a medium with a rough structure include the surface fractal

dimension and the ratio of the average distance between surfaces to the root mean square of the surface height. In this study, we focus on the impact of the surface fractal dimension.

Johnson et al. [35] introduced the term "fractal" to describe the roughness of the pore surface (fluid–structure interface) and to calculate a compensation for the viscous attenuation in porous media caused by this roughness. Researchers have conducted several investigations to model the effect of surface roughness on fluid flow, including those of Brown [34,36], Chen et al. [37], who used the Weierstrass–Mandelbrot function to characterize the self-affine roughness at different scales, and Ghanbarian et al. [38], who proposed that the length and radius of a rough pore can be related through a power-law relationship that was determined by surface fractal dimensions. In their paper, Ghanbarian et al. [38] used the fractal approach to describe the relative permeability for the case of a rough pore. The application of this approach led to a significantly better prediction of the relative permeability when compared to standard approximations and experimental results. Thus, seeing the accuracy of this model, we considered using the tube length–radius relationship to describe the roughness of the tube surface. The originality of this study is that, for the first time, it takes simultaneously into account the effect of the fractal nature of the fluid and that of the tube's surface roughness on the dynamics of the flow, which, according to our knowledge, has not been considered yet. We combine Tarasov's model [32] describing self-similar fluids, with that of Ghanbarian et al. [38] that describes rough "fractal" tube surfaces. This approach is of great interest because it can have a wide range of applications in any field that involves the flow of a fluid that present a self-similar property through a tube exhibiting a "fractal" structure, e.g., fractal fluid dynamics in hydrology [39]. An example of application can be the human bone which is saturated by two main fluids, interstitial fluid and blood [40]. It is common knowledge that blood is made up of many suspended particles as well as proteins, carbohydrates, mineral ions, hormones, carbon dioxide, and blood cells. Blood can exhibit some characteristics of a fractal distribution of various blood components, such as bacteria, viruses, and medications entering the blood. The human bone is a porous medium, in which the fluid–solid interface is not regular in shape and can be considered as fractal as well. A fractal analysis is also crucial in examining the blood circulation in heart and blood vessels [41,42]. A study was recently carried out on the flow of a self-similar, non-Newtonian fluid through a cylindrical pipe. The results showed the effect of the self-similar structure on the rheological behavior of the non-Newtonian fluid [43]. Another study [44] looked at the impact of surface roughness on the flow of a viscous non-Newtonian fluid, using surface fractal dimensions to model the roughness. In this paper, a generalization of the flow of a self-similar Newtonian fluid through a rough-walled pipe is presented. The rest of this paper is organized as follows. In Section 2 we delve into the theoretical models and the mathematical formulations needed for this study. In Section 3, the study of the flow of a Newtonian self-similar fluid through a rough-walled tube is considered. Section 4 presents a discussion of the findings of the study. The paper concludes with a summary of the main points in Section 5.

2. Theoretical Models

2.1. Poiseuille's Law for Viscous Fluid Flow through a Cylindrical Pipe

The well-known Hagen–Poiseuille's law describing the flow of a Newtonian incompressible fluid through a cylindrical pipe can be obtained by solving the following equations:

$$\nabla \cdot \mathbf{v} = 0, \tag{1}$$

$$\frac{d\mathbf{v}}{dt} = \mathbf{f} - \frac{1}{\rho}\nabla p + \nu \Delta \mathbf{v}. \tag{2}$$

Equations (1) and (2) describe the continuity and the momentum equations, respectively. $\mathbf{v} = \mathbf{v}(r, \theta, x)$ is the velocity vector field of the fluid, p refers to the pressure, ρ the density of the fluid, ν the kinematic viscosity, and f the vector field that describes a mass force.

d/dt on the left-hand side of Equation (2) represents the material derivative given by the following relation:

$$\frac{d\mathbf{v}}{dt} = \frac{\partial \mathbf{v}}{\partial t} + (\mathbf{v}.\nabla)\mathbf{v}. \tag{3}$$

For an established laminar flow with respect to the X-axis, solving Equation (2) with boundary conditions $v_x = v_{max}$ at $r = 0$ and $v = 0$ at $r = R$ yields:

$$v_x(r) = -\frac{1}{4\mu}\frac{dp}{dx}R^2\left(1 - \left(\frac{r}{R}\right)^2\right), \tag{4}$$

where $v_x(r)$ represents the velocity distribution in the x direction, R is the pipe radius, and $\mu = \nu/\rho$ is the dynamic viscosity of the fluid. Note that $v_x(r)$ is a function of r only, which is due to the symmetry of the cylindrical pipe and the continuity equation, which simplifies to $\partial v_x/\partial x = 0$. Equation (4) describes the laminar flow of a viscous fluid though a smooth cylindrical pipe. In the next section, we consider the surface of the tube to be rough, with an irregular cross section. The roughness of the tube is modeled using the model from Ghanbarian et al. [38].

2.2. Modeling Surface Roughness Using Fractal Dimensions

Let us assume that the tube surface is rough with an irregular cross section (Figure 3). Ghanbarian et al. [38] proposed that the perimeter of a fractal object could be related to its cross-sectional area:

$$P^2 \propto A^{D_{s2}}, \tag{5}$$

where D_{s2} is the surface fractal dimension $1 \leq D_{s2} < 2$. This exponent determines the smoothness or roughness of the boundary of a cross section. When the boundary is smooth then $D_{s2} = 1$. As for the cross section of the tube A, we can apply the simple assumption $A \propto r_e^2$, where r_e is the mean tube radius or equivalent radius (see Figure 4).

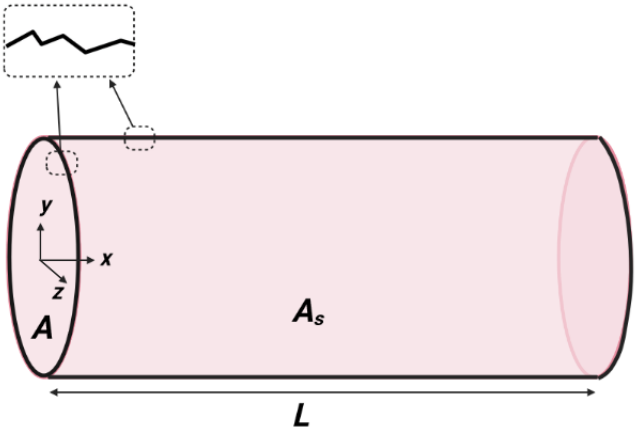

Figure 3. Schematic of a viscous fluid flow through a rough-walled tube.

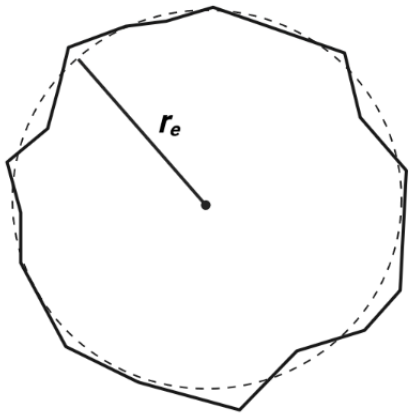

Figure 4. Schematic of the cross section of the tube that displays an irregular pattern.

The Length–Radius Relationship in a Tube

Fractal objects in nature exhibit varying scaling factors and exponents in different directions, which means that they cannot be accurately described using a single fractal dimension. This property, known as scale-invariance, demonstrates the structural anisotropy and self-affinity of these objects [45].

The roughness of the boundary of a tube can be estimated using a three-dimensional surface fractal dimension (D_{s3}) that falls within a range of values between $2 \leq D_{s3} < 3$. The dimension D_{s3} describes the boundary's roughness along the tube structure.

As the three-dimensional surface fractal dimension (D_{s3}) approaches 3, the surface becomes increasingly rough, and for $D_{s3} = 2$ the surface is smooth.

Ghanbarian et al. [38] suggested, for a fractal object, a relationship between the tube surface area A_s and its volume V (Figure 3):

$$A_s^3 \propto V^{D_{s3}}, \tag{6}$$

where:

$$V = L \times A, \tag{7}$$

where L is the tube's length. The surface area (A_s) of the tube can be approximated using the length of the tube (L). The equation for this approximation is as follows:

$$A_s \propto P \times L^{D_r}, \tag{8}$$

where $L^{D_r} = L_f$ is a fractal length which is proportional to the straight line L to the power of the dimension D_r. The latter is a dimension which describes the roughness of the line by representing the power to which the straight line length (L) is raised in order to calculate the fractal length (L_f) (along the x direction in Figure 3).

Combining Equations (7) and (8) with Equations (5) and (6), we get:

$$L \propto r_e^{\frac{2D_{s3}-3D_{s2}}{3D_r-D_{s3}}}. \tag{9}$$

Assuming that the roughness along the tube's structure is isotropic, we then get $D_r = D_{s3} - 1$ [1], which is not necessarily equal to D_{s2}, in particular when the medium is anisotropic [38]. Following this assumption, Equation (9) becomes:

$$L \propto r_e^{\gamma}, \tag{10}$$

where $\gamma = \frac{2D_{s3}-3D_{s2}}{2D_{s3}-3}$. The dimensions $2 \leq D_{s3} < 3$ and $1 \leq D_{s2} < 2$ set boundaries for the behavior described in Equation (10), where $-2 < \gamma \leq 1$. For instance, $\gamma = 1$ represents a nonfractal object with a smooth surface and regular cross section. Note that the nonfractal

case is obtained for $D_{s3} = 2$, $D_{s2} = 1$ and $D_r = 1$. γ can take negative values, therefore L can be inversely proportional to r_e, depending on the values of D_{s2} and D_{s3}.

Equation (10) is valid for anisotropic fractal media [38]. In this case, two dimensions, D_{s3} and D_{s2}, are needed to describe the roughness of the boundary of the tube's cross section.

In the case of an isotropic self-similar fractal medium, the roughness fractal dimension (D_r) can be set as $D_r = D_{s2} = D_{s3} - 1$. With this setup, only one dimension is needed to describe the roughness of the boundary. For an isotropic self-similar fractal medium, one can set $D_r = D_{s2} = D_{s3} - 1$. In this case, only one dimension is needed to describe the roughness of the boundary. Following this assumption, we get the following expression for γ:

$$\gamma = \frac{3 - D_{s3}}{2D_{s3} - 3}. \tag{11}$$

Since $2 \leq D_{s3} < 3$, γ varies between 0 and 1. For a smooth surface, we have $\gamma = 1$, and for a rough surface, $\gamma = 0$. The expression (11) was used in [38] to model the relative permeability in heterogeneous porous media, which led to very accurate results.

We can write:

$$L = c \times r_e^{\gamma}, \tag{12}$$

where c is the constant of proportionality

Next, we study the effect of the fluid's fractal structure on its flow through a tube with a smooth surface. To do this, we use Tarasov's noninteger dimensional space vector calculus to solve the Navier–Stokes equations that describe the laminar flow of a self-similar fluid. This approach allows us to analyze the flow of fluids with a complex, scaling structure.

2.3. Vector Calculus in Noninteger Dimensional Space

Fluids can also possess the property of self-similarity at different scales, which is closely related to the concept of fractals [1]. In fact, self-similarity is considered one of the defining characteristics of fractals. Therefore, a self-similar fluid can be described as a fractal fluid. The mass of a ball region (V_D) of a self-similar "fractal" fluid with radius R follows the relationship $M \propto R^D$, where D is the mass dimension that describes how well the fluid particles fill the ball region. For self-similar fluids, the mass dimension is less than 3 (see Figure 2). We can define S_d to be the boundary of the ball region of fractal dimension d.

The dimension of the ball region of a self-similar fluid (D) and the dimension of the boundary of this region (d) are not related by $d = D - 1$ [26]. As a result, we can define the dimension of a line along the radial direction (α_r) using the following relationship [26]:

$$d = D - \alpha_r. \tag{13}$$

Tarasov [26] proposed a way to extend vector calculus to include noninteger dimensional spaces using these dimensions. This extension includes the definition of first- and second-order operators such as the gradient, divergence, and scalar and vector Laplace operators for noninteger dimensional spaces (NIDS). The scalar and vector fields in this case are assumed to only depend on r due to cylindrical or spherical symmetry (see refs. [26,33] for more details). The divergence and gradient operators in noninteger dimensional space are written in the following form:

$$Div_r^{D,d}\mathbf{u}(r) = \frac{\pi^{(1-\alpha_r)/2}\Gamma((d+\alpha_r)/2)}{\Gamma((d+1)/2)}\left(\frac{1}{r^{\alpha_r-1}}\frac{\partial u_r(r)}{\partial r} + \frac{d}{r^{\alpha_r}}u_r(r)\right), \tag{14}$$

$$Grad_r^{D,d}\phi = \frac{\Gamma(\alpha_r/2)}{\pi^{\alpha_r/2}r^{\alpha_r-1}}\frac{\partial\phi(r)}{\partial r}\mathbf{e}_r, \tag{15}$$

where $\mathbf{u}(r)$ is a vector field and $\phi(r)$ is a scalar field.

Using Equations (14) and (15), we can establish the NIDS Laplacian operators. The vector Laplacian for vector field $\mathbf{u} = u_r(r)\mathbf{e}_r$ has the following expression:

$$\Delta_r^{D,d}\mathbf{u} = Grad_r^{D,d} Div_r^{D,d}\mathbf{u} = A(\alpha_r, d)\left(\frac{1}{r^{2\alpha_r-2}}\frac{\partial^2 u_r}{\partial r^2} + \frac{d+1-\alpha_r}{r^{2\alpha_r-1}}\frac{\partial u_r}{\partial r} - \frac{\alpha_r d}{r^{2\alpha_r}}u_r\right)\mathbf{e}_r, \quad (16)$$

where

$$A(\alpha_r, d) = \frac{\Gamma((d+\alpha_r)/2)\Gamma(\alpha_r/2)}{\pi^{(2\alpha_r-1)/2}\Gamma((d+1)/2)}. \quad (17)$$

The scalar Laplacian for the scalar field $\phi(r)$ is:

$$\Delta_r^{D,d}\phi = Div_r^{D,d} Grad_r^{D,d}\phi = A(\alpha_r, d)\left(\frac{1}{r^{2\alpha_r-2}}\frac{\partial^2 \phi}{\partial r^2} + \frac{d+1-\alpha_r}{r^{2\alpha_r-1}}\frac{\partial \phi}{\partial r}\right). \quad (18)$$

For more details, see ref. [26,27,32,33].

Using these operators we can write the Navier–Stokes and continuity equations for a fractal medium, which describe the behavior of incompressible Newtonian self-similar fluids within the NIDS approach:

$$Div_r^{D,d}\mathbf{v} = 0, \quad (19)$$

$$\frac{d\mathbf{v}}{dt} = f - \frac{1}{\rho}\nabla_x p + \nu\Delta_r^{D,d}\mathbf{v}, \quad (20)$$

where $\mathbf{v}$ is the velocity vector, f the vector field that describes body forces, ρ the fluid density, p the pressure of the fluid, ν the kinematic viscosity, and ∇_x refers to the gradient operator in the x direction. d/dt represents the material derivative:

$$\frac{d\mathbf{v}}{dt} = \frac{\partial \mathbf{v}}{\partial t} + \left(\mathbf{v}, Grad_r^{D,d}\mathbf{v}\right). \quad (21)$$

3. Laminar Flow of a Self-Similar Fluid through a Tube with Rough Walls

When in nature, both a fluid and a rough surface display a fractal structure (e.g., blood flow through blood vessels, any self-similar fluid flow through a rough tube), they can be modeled using noninteger dimensions. Therefore, it is important to understand and investigate the effect of the fractal nature of the fluid and the roughness of the surface on the behavior of the flow. For this purpose, a combination between Ghanbarian et al.'s model, explained in Section 2.2, and Tarasov's model, explained in Section 2.3, is presented. This new approach allows us to study and compare the effects of the fractal structures of the fluid and the surface.

3.1. Velocity Profile of a Self-Similar Fluid

To analyze the flow of a self-similar fluid through a tube with a rough surface (as shown in Figure 5), we must first establish the equations that describe the behavior of the fluid in such case. We can apply Equation (20) for a steady state flow of a self-similar fluid through a cylindrical pipe and parallel to the X-axis (Figure 5). Equation (20) then simplifies to:

$$\Delta_r^{D,d} v_x(r) = \frac{1}{\mu}\frac{dp}{dx}, \quad (22)$$

the velocity component in the x direction ($v_x(r)$) only depends on r due to the symmetry of the cylinder.

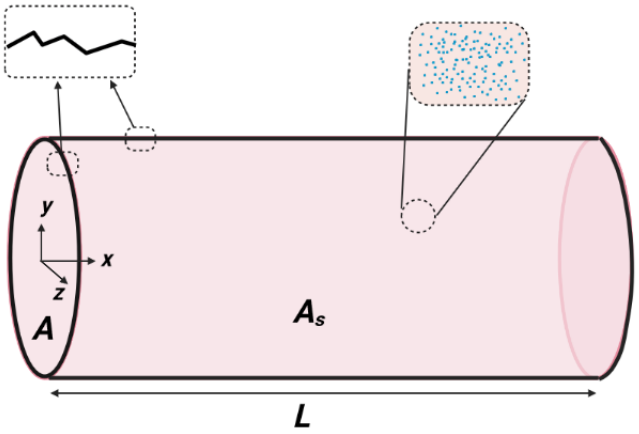

Figure 5. Schematic of self-similar fluid flow through a tube with a rough structure.

Furthermore, since the flow is in the x direction, we define $d \to d_x = d - \alpha_x$, where α_x is the dimension of a line along the x direction. It is assumed that $\alpha_x > 1$ can be used to describe a fractal turbulent flow in a pipe [27].

Using the boundary conditions $v_x(0) = v_{max}$ and $v_x(R) = 0$ for the solution of Equation (22), we find the following velocity profile:

$$v_x(r) = -\frac{1}{2(d_x + \alpha_r)\alpha_r A(d_x, \alpha_r)\mu} \frac{dp}{dx} R^{2\alpha_r} \left(1 - \left(\frac{r}{R}\right)^{2\alpha_r}\right), \tag{23}$$

where $A(d_x, \alpha_r)$ is defined by:

$$A(\alpha_r, d_x) = \frac{\Gamma(\alpha_r/2)\Gamma((d_x + \alpha_r)/2)}{\pi^{(2\alpha_r - 1)/2}\Gamma((d_x + 1)/2)}. \tag{24}$$

We can define the effective dynamic viscosity by:

$$\mu_{eff}(\alpha_r, d_x) = \frac{1}{2}(d_x + \alpha_r)\alpha_r A(\alpha_r, d_x)\mu. \tag{25}$$

Using the above expression, Equation (23) can be written in the following form:

$$v_x(r) = v_{max}(\alpha_r, d_x)\left(1 - \left(\frac{r}{R}\right)^{2\alpha_r}\right), \tag{26}$$

where

$$v_{max}(\alpha_r, d_x) = -\frac{1}{4\mu_{eff}(\alpha_r, d_x)} \frac{dp}{dx} R^{2\alpha_r}. \tag{27}$$

For a nonfractal case ($d_x = \alpha_r = 1$), we get the usual Poiseuille's law (4). Note that in Equation (26), for $\alpha_r < 1$ the velocity profile is proportional to a noninteger power, hence the profile is no longer parabolic. Notice that $\frac{dv_x(r)}{dr} \propto r^{2\alpha_r - 1}$. For the velocity profile $v_x(r)$ to represent a physical solution, the power $2\alpha_r - 1$ needs to be a positive number, otherwise the gradient of v_x diverges. Thus, this gives limits to the values permitted for α_r. Consequently, we get $0.5 < \alpha_r \leq 1$.

For a rough surface, we use the length–radius relationship (12) established in Section 3. In order to more easily analyze the flow through tubes that have irregular cross sections, we use the equivalent radius (r_e) (see Figure 4), hence

$$R \to r_e.$$

Considering this assumption and substituting the tube length–radius relationship (12) into Equation (26) yields:

$$v_x(r) = \frac{\Delta p}{4\mu_{eff}(d_x, \alpha_r)c} r_e^{2\alpha_r - \gamma} \left(1 - \left(\frac{r}{r_e}\right)^{2\alpha_r}\right). \tag{28}$$

Equation (28) is a velocity distribution that contains fractal dimensions, which describes the flow of a self-similar fluid through a tube having a rough surface. For $D_{s3} = 2$ and $d_x = \alpha_r = 1$, we get the usual Poiseuille's law for a nonfractal case.

For an isotropic self-similar fractal medium, we have $D_r = D_{s2} = D_{s3} - 1$, where

$$\gamma = \frac{3 - D_{s3}}{2D_{s3} - 3}.$$

Since $2 \leq D_{s3} < 3$, γ varies between 0 and 1. For $\gamma = 1$, we get a smooth surface, and for $\gamma = 0$ the surface is extremely rough.

3.2. Fluid Discharge

The new expression of the velocity profile (28) can be used to obtain the fractal fluid discharge. Since self-similar fluids are described as a homogeneous continuum that can be quantified by fractal dimensions, we can use the integration in a noninteger dimensional space [46]:

$$\int_{R^D} d^D\mathbf{r}\phi(\mathbf{r}) = \frac{2\pi^{(D-1)/2}}{\Gamma((D-1)/2)} \int_0^\infty dr r^{D-1} \int_0^\pi d\theta sin^{D-2}\theta\phi(r,\theta), \tag{29}$$

where $d^D\mathbf{r}$ represents the volume element in a noninteger dimensional space. Having that

$$\int_0^\pi d\theta sin^{D-2}\theta = \frac{\pi^{1/2}\Gamma((D-1)/2)}{\Gamma(D/2)}, \tag{30}$$

the expression of the fluid discharge Q can be written as

$$Q = \frac{2\pi^{d/2}}{\Gamma(d/2)} \int_0^{r_e} r^{d-1} v_x(r) d, \tag{31}$$

with d being a noninteger dimension that characterizes the cross section. Using Equation (28) for the velocity profile $v_x(r)$, for simplification, we can consider $\alpha_r = 1$. We then get:

$$Q = \frac{4\pi^{d/2}\Delta p}{\Gamma(d/2)\mu c(d+2)d^2} r_e^{d+2-\gamma}. \tag{32}$$

For $d = D - 1$, we get:

$$Q = \frac{2\pi^{(D-1)/2}\Delta p}{\Gamma((D-1)/2)\mu c(D+1)(D-1)^2} r_e^{D+1-\gamma}. \tag{33}$$

Using an effective viscosity:

$$\mu_{eff} = \frac{\pi^{(3-D)/2}}{16}(D+1)(D-1)^2\Gamma((D-1)/2)\mu, \tag{34}$$

we get the final expression of the fluid discharge:

$$Q = \frac{\pi}{8}\frac{\Delta p}{c\mu_{eff}} r_e^{D+1-\gamma}. \tag{35}$$

Notice that for the nonfractal case ($D = 3$ and $D_{s3} = 2$), we get the usual Hagen–Poiseuille's equation for the fluid discharge:

$$Q = \frac{\pi}{8}\frac{\Delta p}{\mu L}R^4, \tag{36}$$

where R is the the radius of a tube with a circular cross section.

In comparison with Hagen–Poiseuille's equation, the new expression of the fluid discharge (35) contains fractal dimensions D and D_{s3}, and an effective viscosity μ_{eff}. The fluid discharge (35) is proportional to the radius to the power of $(D + 1 - \gamma)$ instead of R^4, and for the fractal case, the power $(D + 1 - \gamma)$ is less than 4.

3.3. Darcy's Friction Factor

It would also be interesting to see how the roughness affects the behavior of the fluid, by calculating the friction factor for the fractal case. The friction factor can be expressed using the Darcy–Weisbach equation [47] as follows:

$$f = \frac{8\tau_w}{\rho\bar{v}^2}, \tag{37}$$

where τ_w is the wall's shear stress and $\bar{v}$ is the mean velocity. Since we have the expression of the velocity distribution for the fractal case (28), we can easily obtain τ_w and $\bar{v}$ for such a case:

$$\tau_w = -\mu\frac{dv_x(r)}{dr}|_{r=r_e} \tag{38}$$

$$\bar{v} = \frac{1}{S_d}\int_0^{r_e} v_x(r)d^d r, \tag{39}$$

where S_d is the surface in a $d = D - 1$ dimensional cross section with radius r_e, with

$$S_d = \int_0^{r_e} d^{D-1}r = \frac{2\pi^{(D-1)/2}}{\Gamma((D-1)/2)}\frac{r_e^{D-1}}{(D-1)}. \tag{40}$$

The final expressions of τ_w and $\bar{v}$ are as follows:

$$\tau_w = \frac{\Delta p}{(D-1)c}r_e^{1-\gamma} \tag{41}$$

$$\bar{v} = \frac{\Delta p}{c\mu\Gamma((D-1)/2)(D+1)(D-1)}r_e^{2-\gamma}. \tag{42}$$

Replacing Equations (41) and (42) in Equation (37), we get the following for the Darcy friction factor:

$$f = \frac{8[\Gamma((D-1)/2)(D+1)]^2(D-1)\mu^2 c}{\rho\Delta p}r_e^{\gamma-3}. \tag{43}$$

If we set $D = 3$ and $D_{s3} = 2$, we get the standard equation for the Darcy friction factor for the laminar flow of a viscous fluid:

$$f = \frac{64}{\Re_e}, \tag{44}$$

where $\Re_e$ is the Reynolds number.

The new expression of the friction factor (43) contains fractal dimension D describing the self-similarity of the fluid and surface fractal dimension D_{s3} describing the roughness of the surface, that is, even the self-similarity of the fluid has an influence on how the surface affects the flow dynamics.

The different formulas found in this section are plotted numerically, and fully discussed in what comes next.

4. Results and Discussion

To describe the fractal structure of the tube surface, it is critical to understand the tube length–radius relationship discussed in earlier sections. The relationship $L \propto r_e^{\gamma}$ describes the roughness of the surface for anisotropic and isotropic media. To simplify the analysis, an isotropic case is assumed, where only the dimension D_{s3} is required to determine the roughness of the tube's surface. In this case we get $\frac{3-D_{s3}}{2D_{s3}-3}$. When the medium is anisotropic, modern approaches such as 3-D image analysis should be used to determine the roughness parameters (e.g., D_{s2} and D_{s3}). The range of values of D_{s3} $(2 \leq D_{s3} < 3)$ yields that γ varies between 1 and 0. A value of $D_{s3} = 2 (\gamma = 1)$ represents a smooth surface, and a value of $D_{s3} = 3$ $(\gamma = 0)$ corresponds to an extremely rough surface, which completely blocks the flow of the fluid. The velocity distribution (28) is proportional to the power $2\alpha_r$, which means that the flow dynamics are strongly influenced by the fractal nature of the fluid. The fractal dimensions α_r and d_x reflect the self-similarity present in the fluid, and the fluid is fractal when $\alpha_r < 1$ and $d_x < 1$. Additionally, Equation (28) shows that to have zero viscous shear effects at the center of the tube, the velocity gradient must be zero at $r = 0$, which places a limit on the values of the radial dimension α_r and gives us $0.5 < \alpha_r \leq 1$.

A very important aspect to point out is that the velocity distribution (28), the fluid discharge (35), and the friction factor (43) are new expressions that contain fractal dimensions, which are theoretically based. These new expressions are very interesting because they can prove useful in the prediction of the behavior of complex fluids that are in contact with a surface that present an irregular pattern. A very good example of application would be the human bone, which is saturated by interstitial fluid and blood. The latter is considered to be a self-similar fluid, and the human bone is a porous medium, where the pores does not have a regular shape, nor a smooth solid–fluid interface. Likewise, the models that exist today do not consider the roughness of the solid–fluid interface.

Figures 6 and 7 plot the velocity profile defined by Equation (28) and demonstrate some interesting results. For instance, in Figure 6, it appears that the fractal nature of the fluid plays a significant role in the flow dynamics. By comparing (a) $\alpha_r = 1$ to (b) $\alpha_r = 0.55$, we see that the velocity profile becomes narrower and has a higher amplitude. This is because a fluid with a higher degree of self-similarity becomes thicker near the walls, leading to a narrower velocity distribution and an increase in the velocity profile's amplitude in the center of the tube due to the conservation of momentum. In contrast, Figure 7 shows that when the surface becomes rougher (from (a) a smooth surface $(D_{s3} = 2)$ to (b) a rough surface $(D_{s3} = 2.9)$), the velocity profile's amplitude decreases by a factor of 10^2. This is expected because D_{s3} is a measure of surface roughness and an increase in D_{s3} leads to an increase in friction losses. However, unlike the fractal nature of the fluid, surface roughness does not affect the velocity profile's shape. Therefore, it is safe to conclude that the effect of the self-similarity of the fluid is dominant compared to that of the surface roughness. Another interesting result, is that the behavior of self-similar fluids is very similar to that of non-Newtonian fluids, more specifically, shear-thickening (dilatant) fluids. The similarity between the two is highlighted in Figure 8, which plots the velocity profile defined by Equation (28) for $\alpha_r = 0.9$ and $D_{s3} = 2.223$, compared with the velocity distribution of a shear-thickening fluid modeled by the Ostwald–de Waele relationship (power-law model) with $n = 1.5$. The number n is called the power-law index, which is an empirical number specific to the type of the fluid. A fluid is classified as pseudoplastic or shear-thinning when the power n is less than one, as Newtonian when n is equal to one, and as dilatant or shear-thickening when n is greater than one. As the figure illustrates, it is very clear that shear-thickening fluids and self-similar fluids have the same behavior. We assume that the new expression of the velocity profile we found can also predict the rheological behavior of shear-thickening fluids. This is interesting because the models that describe

these fluids are, generally speaking, empirical or semi-empirical models (e.g., a power-law model), on the other hand, Equation (28) is a theory-based formula. Nevertheless, the exact interpretation of these results need further extensive experimental and theoretical investigations, which will be considered for future studies.

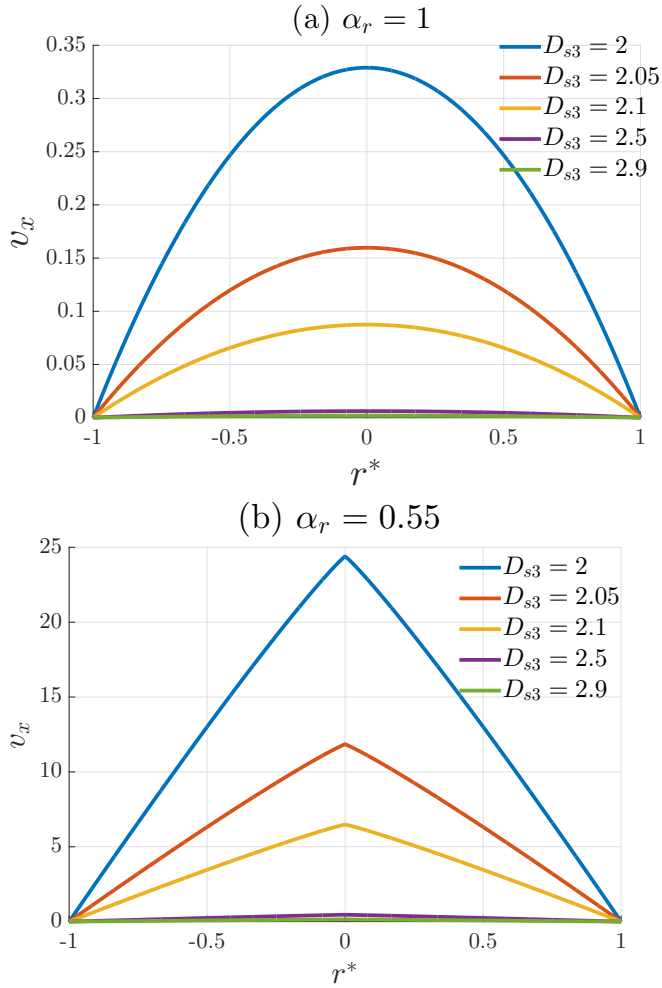

Figure 6. Plots of velocity profiles defined by Equation (28), with $r^* = r/r_e$, $d_x = 0.9$, $\Delta p = 25$ Pa, $\mu = 10^{-3}$ Pa.s, and $c = 100$ m$^{1-\gamma}$.

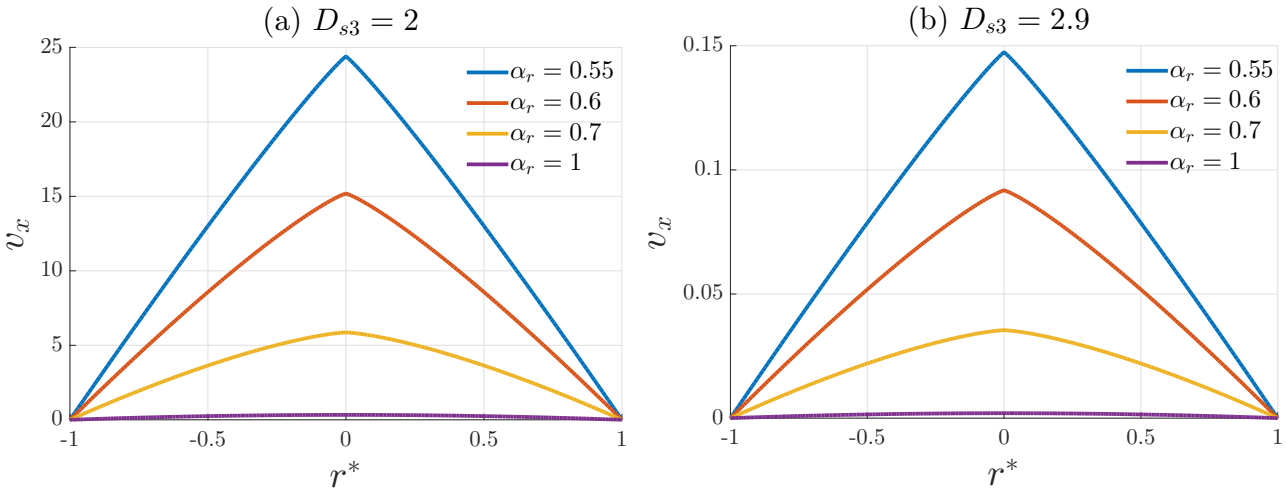

Figure 7. Plots of velocity profiles defined by Equation (28), with $r^* = r/r_e$, $d_x = 0.9$, $\Delta p = 25$ Pa, $\mu = 10^{-3}$ Pa.s, and $c = 100$ m$^{1-\gamma}$.

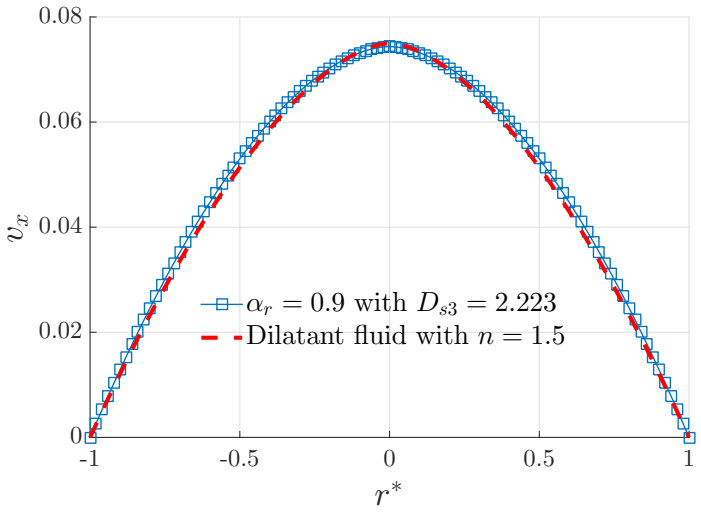

Figure 8. Plots of the velocity profile defined by Equation (28) for $\alpha_r = 0.9$ and $D_{s3} = 2.223$, compared with the velocity distribution of a dilatant fluid with index $n = 1.5$, with $r^* = r/r_e$, $d_x = 0.9$, $\Delta p = 25$ Pa, $\mu = 10^{-3}$ Pa.s, and $c = 100\ \mathrm{m}^{1-\gamma}$.

Figure 9 plots the fractal fluid discharge with radial dimension $\alpha_r = 1$ with respect to the surface fractal dimension D_{s3} for (a) $1 < D \leq 3$ and (b) $0 < D < 1$. Figure 9a illustrates that the flow decreases as the surface fractal dimension increases, which is obvious and already discussed earlier in this section. In contrast, Figure 9b demonstrates a very interesting result for fluids with mass dimension $D < 1$. We can see that the fractal fluid discharge Q is negative. The same thing can be observed in Figure 10, which plots the friction factor with respect to the surface fractal dimension S_{s3} for different values of the mass dimension D. We can see that for $D < 1$, the friction factor is negative. Keep in mind that $D < 1$ corresponds to a very high degree of self-similarity present in the fluid. The negative values of the fluid discharge and the friction factor is due to the effective viscosity being negative for values of $D < 1$, which is shown in Figure 11. Experiments have shown that it is possible to achieve negative viscosity, and that this can have significant effects. Researchers from Paris-Sud University found that certain types of bacteria can change the viscosity of a liquid by altering the fluid's hydrodynamic properties through their swimming motion. It was predicted that these microorganisms could reduce the viscosity of a fluid to zero under certain conditions, resulting in a superfluid. By providing the bacteria with extra nutrients, the researchers observed not only a viscosity of zero, but also negative values of viscosity, as measured by a rheometer (for more details see ref. [48]). Interestingly enough, based on the definition of self-similarity, bacteria suspensions can also exhibit some characteristics of a fractal distribution similar to self-similar fluids.

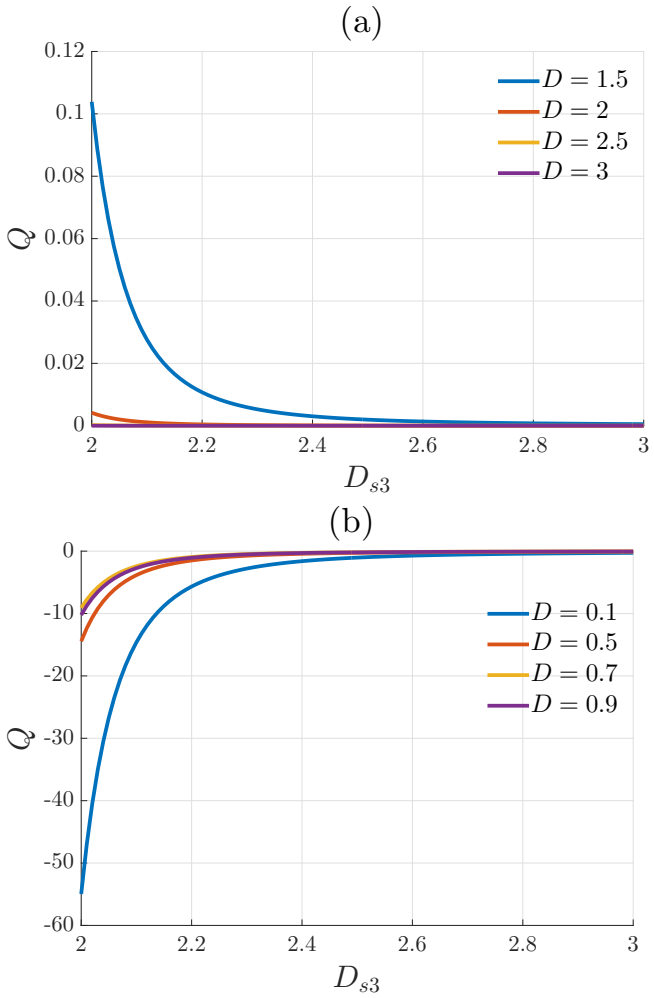

Figure 9. Plots of the fractal fluid discharge Q defined by Equation (35) with respect to the surface fractal dimension D_{s3} for different values of the mass dimension D, for (**a**) $1 < D \leq 3$, and (**b**) $0 < D < 1$. $\Delta p = 25$ Pa, $\mu = 10^{-3}$ Pa.s, and $c = 100$ m$^{1-\gamma}$.

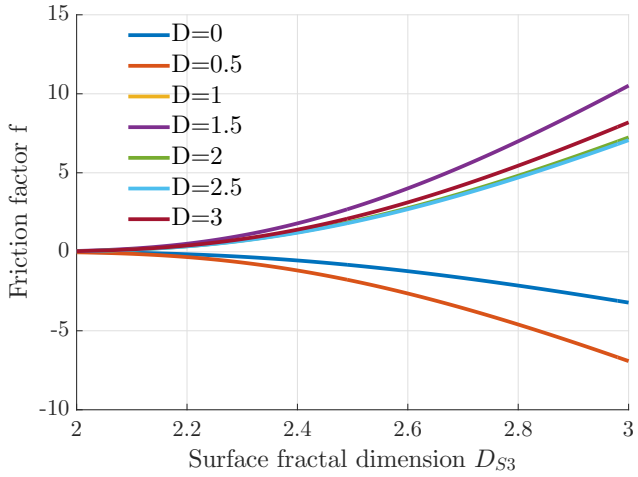

Figure 10. Plots of the Darcy friction factor defined by Equation (43) with respect to the surface fractal dimension D_{s3} for different values of the mass dimension D, with $\Delta p = 25$ Pa, $\mu = 10^{-3}$ Pa.s, and $c = 100$ m$^{1-\gamma}$.

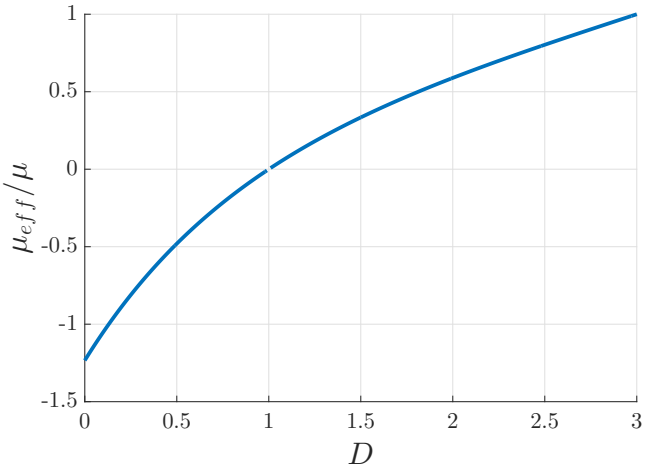

Figure 11. Plots of the effective viscosity defined by Equation (34) with respect to the mass dimension D.

5. Concluding Remarks

To conclude, the use of fractal dimensions to describe the fractal structures of fluids and surfaces was presented. The main objective of this study was to combine and compare the effects of the fractal nature of the fluid and the tube surface, which had not been considered before. By using a fractal approach, we found new expressions for the velocity profile, the fluid discharge, and the friction factor. Our findings showed some very interesting results. The fractal dimensions describing a self-similar fluid and those describing the pipe's surface roughness affected differently the flow of the fluid. The fractal structure of a fluid affected both the shape and the amplitude of the velocity profile. On the other hand, the surface roughness using fractal dimensions affected only the amplitude, meaning that the effect of the fractality of the fluid was dominant compared to that of the surface roughness. It is also important to mention that this study qualitatively demonstrated that self-similar fluids and shear-thickening fluids had the same rheological behavior. Nevertheless, the exact interpretations need further studies. We anticipate that this approach will spur further theoretical and experimental investigations on the study of the flow dynamics of fractal fluids through a rough surface, for instance, a fractal fluid flow through a porous medium (e.g., bones saturated by blood), where the pores are considered to be rough-walled tubes.

Author Contributions: Writing—original draft preparation, A.B., Z.E.A.F., Z.L., N.O.O., M.F., E.O. and C.D.; analysis, analytical calculations, and processing of results, A.B., Z.E.A.F., Z.L., N.O.O., M.F., E.O. and C.D.; Writing—review and editing, A.B., Z.E.A.F., Z.L., N.O.O., M.F. and C.D.; resources, Z.E.A.F., Z.L., N.O.O., M.F., E.O. and C.D. All authors have read and agreed to the published version of the manuscript.

Funding: This research received no external funding.

Institutional Review Board Statement: Not applicable.

Informed Consent Statement: Not applicable.

Data Availability Statement: Not applicable.

Conflicts of Interest: The authors declare no conflict of interest.

References

1. Mandelbrot, B.B. *The Fractal Geometry of Nature*; WH freeman: New York, NY, USA, 1982.
2. Mandelbrot, B.B. How long is the coast of Britain? Statistical self-similarity and fractional dimension. *Science* **1967**, *156*, 636–638. [CrossRef] [PubMed]
3. Bizzarri, M.; Giuliani, A.; Cucina, A.; Anselmi, F.D.; Soto, A.M.; Sonnenschein, C. Fractal analysis in a systems biology approach to cancer. *Semin. Cancer Biol.* **2011**, *21*, 175–182. [CrossRef] [PubMed]

4. Mambetsariev, I.; Mirzapoiazova, T.; Lennon, F.; Jolly, M.K.; Li, H.; Nasser, M.H.; Vora, L.; Kulkarni, P.; Batra, S.K.; Salgia, R. Small cell lung cancer therapeutic responses through fractal measurements: From radiology to mitochondrial biology. *J. Clin. Med.* **2019**, *8*, 1038. [CrossRef] [PubMed]
5. Avşar, E. Contribution of fractal dimension theory into the uniaxial compressive strength prediction of a volcanic welded bimrock. *Bull. Eng. Geol. Environ.* **2020**, *79*, 3605–3619. [CrossRef]
6. Xie, H. *Fractals in Rock Mechanics*; CRC Press: Boca Raton, FL, USA, 2020.
7. Pierre, S.; Jean, F.R. On the validity of fractal dimension measurements in image analysis. *J. Vis. Commun. Image Represent.* **1996**, *7*, 217–229.
8. Emanuel, G. Primality, fractality, and image analysis. *Entropy* **2019**, *21*, 304.
9. Caicedo-Ortiz, H.E.; Santiago-Cortes, E.; Lopez-Bonilla, J.; Castaneda, H.O. Fractal dimension and turbulence in Giant HII Regions. *J. Phys. Conf. Ser.* **2015**, *582*, 012049. [CrossRef]
10. Gaite, J. The fractal geometry of the cosmic web and its formation. *Adv. Astron.* **2019**, *2019*, 6587138. [CrossRef]
11. Petros, M.; Alexandros, P. Fractal dimensions of speech sounds: Computation and application to automatic speech recognition. *J. Acoust. Soc. Am.* **1999**, *105*, 1925–1932.
12. Berbiche, A.; Fellah, M.; Fellah, Z.E.A.; Ogam, E.; Mitri, F.G.; Depollier, C. Transient acoustic wave in self-similar porous material having rigid frame: Low frequency domain. *Wave Motion* **2017**, *68*, 12–21. [CrossRef]
13. Fellah, M.; Fellah, Z.E.A.; Berbiche, A.; Ogam, E.; Mitri, F.G.; Depollier, C. Transient ultrasonic wave propagation in porous material of non-integer space dimension. *Wave Motion* **2017**, *72*, 276–286. [CrossRef]
14. Fellah, Z.E.A.; Fellah, M.; Ogam, E.; Berbiche, A.; Depollier, C. Reflection and transmission of transient ultrasonic wave in fractal porous material: Application of fractional calculus. *Wave Motion* **2021**, *106*, 102804. [CrossRef]
15. Fellah, Z.E.A.; Fellah, M.; Ongwen, N.O.; Ogam, O.; Depollier, C. Acoustics of Fractal Porous Material and Fractional Calculus. *Mathematics* **2021**, *9*, 1774. [CrossRef]
16. Hills, B.P.; Manoj, P.; Destruel, C. NMR Q-space microscopy of concentrated oil-in-water emulsions. *Magn. Reson. Imaging* **2000**, *18*, 319–333. [CrossRef]
17. Shui, H.; Zhou, H. Viscosity and fractal dimension of coal soluble constituents in solution. *Fuel Process. Technol.* **2004**, *85*, 1529–1538. [CrossRef]
18. Shiyan, A.A. Viscosity for fractal suspensions: Dependence on fractal dimensionality. *Phys. Lett. A* **1996**, *220*, 117–119. [CrossRef]
19. Demmie, P.N.; Ostoja-Starzewski, M. Waves in fractal media. *J. Elast.* **2011**, *104*, 187–204. [CrossRef]
20. Joumaa, H.; Ostoja-Starzewski, M. Acoustic-elastoodynamic interaction in isotropic fractal media. *Eur. Phys. J. Spec. Top.* **2013**, *222*, 1951–1960. [CrossRef]
21. Ostoja-Starzewski, M. Electromagnetism on anisotropic fractals. *Z. Angew. Math. Phys. (J. Appl. Math. Mech.)* **2013**, *64*, 381–390.
22. Ostoja-Starzewski, M.; Li, J.; Joumaa, H.; Demmie, P.N. From fractal media to continuum mechanics. *Z. Angew. Math. Phys.* **2014**, *94*, 373–401. [CrossRef]
23. Balankin, A.S. Steady laminar flow of fractal fluids. *Phys. Lett. A* **2017**, *381*, 623–628. [CrossRef]
24. Balankin, A.S.; Bory-Reyes, J.; Shapiro, M. Towards a physics on fractals: Differential vector calculus in three-dimensional continuum with fractal metric. *Physica A* **2016**, *444*, 345–359. [CrossRef]
25. Balankin, A.S. Fractional space approach to studies of physical phenomena on fractals and in confined low-dimensional systems. *Chaos Solitons Fractals* **2020**, *132*, 109572. [CrossRef]
26. Tarasov, V.E. Vector calculus in non-integer dimensional space and its applications to fractal media. *Commun. Nonlinear Sci. Numer. Simul.* **2015**, *20*, 360–374. [CrossRef]
27. Tarasov, V.E. Flow of fractal fluid in pipes: Non-integer dimensional space approach. *Chaos Solitons Fractals* **2014**, *67*, 26–37. [CrossRef]
28. Hooft, G.; Veltman, M. Regularization and renormalization of gauge fields. *Nucl. Phys. B* **1972**, *44*, 189–213. [CrossRef]
29. Leibbrandt, G. Introduction to the technique of dimensional regularization. *Rev. Modern Phys.* **1975**, *47*, 849–876. [CrossRef]
30. Wilson, K.G.; Fisher, M.E. Critical exponents in 3.99 dimensions. *Phys. Rev. Lett.* **1972**, *28*, 240–243. [CrossRef]
31. Wilson, K.G. Kogut, J. The renormalization group and the ϵ expansion. *Phys. Rep.* **1974**, *12*, 75–199. [CrossRef]
32. Tarasov, V.E. Poiseuille equation for steady flow of fractal fluid. *Int. J. Mod. Phys. B* **2016**, *30*, 1650128. [CrossRef]
33. Tarasov, V.E. Anisotropic fractal media by vector calculus in non-integer dimensional space. *J. Math. Phys.* **2014**, *55*, 083510. [CrossRef]
34. Brown, S.R. Fluid flow through rock joints: The effect of surface roughness. *J. Geophys. Res. Solid Earth* **1987**, *92*, 1337–1347. [CrossRef]
35. Johnson, D.L.; Koplik, J.; Dashen, R. Theory of dynamic permeability and tortuosity in fluid-saturated porous media. *J. Fluid Mech.* **1987**, *176*, 379–402. [CrossRef]
36. Brown, S.R.; Stockman, H.W.; Reeves, S.J. Applicability of the Reynolds equation for modeling fluid flow between rough surfaces. *Geophys. Res. Lett.* **1995**, *22*, 2537–2540. [CrossRef]
37. Chen, Y.; Zhang, C.; Shi, M.; Peterson, G.P. Role of surface roughness characterized by fractal geometry on laminar flow in microchannels. *Phys. Rev. E* **2009**, *80*, 026301. [CrossRef]
38. Ghanbarian, B.; Hunt, A.G.; Daigle, H. Fluid flow in porous media with rough pore-solid interface. *Water Resour. Res.* **2016**, *52*, 2045–2058. [CrossRef]

39. Benson, D.A.; Meerschaert, M.M.; Revielle, J. Fractional calculus in hydrologic modeling: A numerical perspective. *Adv. Water Resour.* **2013**, *51*, 479–497. [CrossRef]
40. Cowin, S.C.; Cardoso, L. Blood and Interstitial flow in the hierarchical pore space architecture of bone tissue. *J. Biomech.* **2015**, *48*, 842–854. [CrossRef]
41. Gabrys, E.; Rybaczuk, M.; Kedzia, A. Blood flow simulation through fractal models of circulatory system. *Chaos Solitons Fractals* **2006**, *27*, 1–7. [CrossRef]
42. Jayalalithaa, V.G.; Shanthoshini Devihab, V.; Uthayakumar, R. Fractal model for blood flow in cardiovascular system. *Comput. Biol. Med.* **2008**, *38*, 684–693. [CrossRef]
43. Bouchendouka, A.; Fellah, Z.E.A.; Larbi, Z.; Ongwen, O.N.; Ogam, E.; Fellah, M.; Depollier, C. Flow of a self-similar non Newtonian fluid using fractal dimensions. *Fractal Fract.* **2022**, *6*, 582. [CrossRef]
44. Bouchendouka, A.; Fellah, Z.E.A.; Larbi, Z.; Louna, Z.; Ogam, E.; Fellah, M.; Depollier, C. Fractal Analysis of a Non-Newtonian Fluid Flow in a Rough-Walled Pipe. *Materials* **2022**, *15*, 3700. [CrossRef] [PubMed]
45. Carr, J.R. Statistical self-affinity, fractal dimension, and geologic interpretation. *Eng. Geol.* **1997**, *48*, 3–4. [CrossRef]
46. Stillinger, F.H. Axiomatic basis for spaces with noninteger dimensions. *J. Math. Phys.* **1977**, *18*, 1224–1234. [CrossRef]
47. Brown, G.O. Chapter: The history of the Darcy-Weisbach equation for pipe flow resistance. *Proc. Environ. Water Resour. Hist.* **2002**, *38*, 34–43.
48. López, H.M.; Gachelin, J.; Douarche, C.; Auradou, H.; Clément, E. Turning Bacteria Suspensions into Superfluids. *Phys. Rev. Lett.* **2015**, *115*, 028301. [CrossRef]